International Journal of Pressure Vessels and Piping 198 (2022) 104662

Contents lists available at ScienceDirect

International Journal of Pressure Vessels and Piping

journal homepage: www.elsevier.com/locate/ijpvp

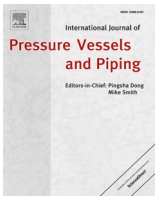

Mechanical responses of L450 steel under biaxial loading in the presence of the stress discontinuity

Shuai Wang [a,b], Cheng Hou [c], Bin Wang [b,*], Guiyi Wu [d], Xueling Fan [c], He Xue [e]

[a] School of Safety Science and Engineering, Xi'an University of Science and Technology, Xi'an, 710054, China
[b] Department of Mechanical and Aerospace Engineering, Brunel University, London, UB8 3PH, UK
[c] State Key Laboratory for Strength and Vibration of Mechanical Structures, Xi'an Jiaotong University, Xi'an, 710049, China
[d] Centre of Excellence for Advanced Materials, Dongguan, 523808, China
[e] School of Mechanical Engineering, Xi'an University of Science and Technology, Xi'an, 710054, China

ARTICLE INFO

Keywords:
Stress discontinuity
Biaxial loading
Lüders band
Yielding

ABSTRACT

The Lüders plateau behaviour is a phenomenon of stress discontinuity associated with strain localisation which can affect the fracture behaviour of mild steel subjected to plastic strains. Together with experimental studies of biaxial loading tests with digital image correlation (DIC), this work considers the effect of stress discontinuity on the mechanical behaviour of L450 steel subjected to biaxial loading, using the so-called "up-down-up" (UDU) constitutive model in finite element analyses (FEA) of cruciform specimens. The softening modulus of the UDU model and the stress ratio were found to significantly affect the simulated evolution of the Lüders band. A method has been proposed to use appropriate UDU parameters which capture the characters of the Lüders bands in biaxial loading conditions. Based on the selected parameters, the formation of the Lüders bands illustrated in the stress distribution and the Lüders plateau in the force-displacement were studied over the full range of the loading ratio under biaxial loading conditions.

1. Introduction

Pipelines are essential components commonly employed in various industrial applications, including the nuclear, oil and gas industries. With the growing energy demand, more pipelines are being designed and constructed to operate in harsh and remote environments, which include seismically-active and permafrost regions [1,2]. The pipelines operating in these environments are affected by potential large plastic deformations, posing threats to pipeline management and safe operation [3].

Although pipelines are rarely designed for plastic straining, defects in pipeline (e.g. crack) will cause stress concentration and local area plastic deformation [4,5]. Furthermore, these critical components are frequently applied to plastic straining during the installation process, such as S-lay, J-lay and reel-lay for offshore applications [6,7]. During the plastic straining phase, the deformation behaviour of pipelines is often complicated by a yielding behaviour of the material, known as the yield discontinuity, which is usually manifested by a yield plateau or the Lüders plateau [8,9]. The effect of yield discontinuity in the pipeline has been an ongoing issue that has received attention in recent years [10,11].

The Lüders plateau in the stress-strain curve, commonly regarded as having been first reported by Piobert and Lüders, is a material instability frequently encountered in mild steels [12,13]. This material characteristic is known as the result of dislocation pinning accounting for the upper yield stress, and dislocation release and multiplication leading to the subsequent stress drop [14,15]. The Lüders plateau is manifested by the propagation of localised deformation bands (termed as the Lüders bands) during uniaxial tensile tests [16,17]. The localisation band is usually initiated at stress concentrators, such as the shoulder of a tensile specimen, and then propagates with an inclination angle of approximately from 45° to 55° to the loading axis [18–20]. Previous studies have found that the Lüders plateau will affect the structural instabilities and deformation capacity of steel pipes [21–23].

Operational pipelines and pressure vessels are usually pressurized, leading to biaxial loading conditions [24,25]. A lot of research have been carried out, looking at surface cracks in pressure pipes with biaxial loading condition [26,27]. The effect of biaxial stressing on J-integral of a finite plate containing a through-thickness crack and subjected to

Abbreviations: DIC, digital image correlation; FBC, free boundary condition; FEA, finite element analysis; UDU, up-down-up models.

* Corresponding author.
E-mail address: bin.wang@brunel.ac.uk (B. Wang).

https://doi.org/10.1016/j.ijpvp.2022.104662
Received 13 December 2021; Received in revised form 22 February 2022; Accepted 28 March 2022
Available online 4 April 2022

Nomenclature

D_x	displacement on X-axis	T	time
D_y	displacement on Y-axis	t_a	thickness of specimen loading arms
E	Young's modulus	t_s	thickness of specimen centre sag
E_L	softening modulus of the softening segment in UDU stress-strain mode	V_x	loading rate on X-axis
		V_y	loading rate on Y-axis
		$\triangle e_L$	the length of Lüders plateau
$\overline{E}_L$	normalized softening modulus	ν	Poisson's ratio
F	force on the end of specimen	ε	strain
R_{eL}	plateau stress	σ	stress
s_{ly}	lower yield stress of the UDU stress-strain model	σ_0	yield strength
s_{uy}	upper yield stress of the UDU stress-strain model	σ_{ly}	lower yield stress of the material
		σ_{uy}	upper yield stress of the material

biaxial stresses were investigated by Wang et al. [28]. They found that the length of yielding or Lüders plateau is a very important factor affecting the J-integral path dependency. A positive correlation of the length of Lüders plateau with the path dependence of the J-integral. Østby has proposed a method for calculating the crack driving force for pipes with surface crack [29], the results show that their equation can get accurate results for engineering calculations in most cases. However, the effect of Lüders plateau on the applied driving force was lack of consideration in their investigation.

Biaxial loading can cause failure of the material at loads much less than that determined by uniaxial testing methods [30]. Limited by the number of apparatus, relatively few experimental investigations have been carried out to characterize sheet metals under biaxial tension. By designing a biaxial test machine, various types of cruciform specimens at both small and large strains were tested for each axis by Makinde et al. Their research was used to develop an optimum specimen for low strains [31]. Kuwabara et al. designed biaxial tensile-testing apparatus to study the elastic and plastic deformation behaviour of cold rolled low-carbon steel under biaxial loading conditions. The result shows that the measured flow stresses for ultra low carbon steel under biaxial loading were in good agreement with the predicted by Hosford's yield criterion [32]. Naumenko and Atkins performed biaxial tensile tests on pre-cracked high-strength low-hardening aluminium specimens at various in-plane constraint states. Their study focus on determining the crack tip opening geometry when parameters such as the specimen geometry, specimen size and biaxiality ratio were varied [33]. Nonetheless, most of the previous research used uniaxial loading to study the phenomenon of stress discontinuity [34–37]. There are a limited number of studies available in the public domain on the phenomenon of stress discontinuity under biaxial loading. In an earlier report, Heyer and Newby studied the response of low carbon steel sheets to biaxial tension forces by using hydraulic bulge type cup tests, which is an approximate approach to pure biaxial stretching [38]. The results show that the Lüders strain depressions in the sheet surface could cause premature failure in the hydraulic bulge type cup tests, and the premature failure can be reduced by temper rolling and lubrication. 1045 steel under torsion and combined tension and torsion was investigated by Zhang and Jiang using strain gauges [39]. Their results showed that the Lüders fronts were approximately parallel to the plane of maximum shear in monotonic tension, torsion, and biaxial tension–torsion with a constant axial load. They also found that multiple Lüders bands can be formed simultaneously during the propagation of the bands. Lüders band formation in Al–Mg alloy sheets was investigated by Minoda et al. under biaxial loading with the stress ratio ranging from 8:0 (uniaxial loading) to 8:8 [40]. It was reported that the Lüders band phenomenon was observed in stress ratios from 8:0 and 8:6, but not beyond. Cam et al. studied the Spatio-temporal distribution of heat produced by Portevin-Le-Chatelier (PLC) bands formed in Al–Mg alloy subjected to equal biaxial tensile loading [41], and earlier studies have shown that the PLC bands can be compared to the smooth propagating Lüders bands in steels [42]. Using an infrared camera, they found that the force-time curves in the two perpendicular directions were almost identical under equal biaxial loading conditions. The PLC bands were formed in a cross shape and propagated from the centre of the specimen to the borders with increasing loading. Recently, Hou et al. did a similar trial for investigating the plastic instabilities in the aluminium alloy sheet under three different stress states (uniaxial tension, biaxial tension with a load ratio of 1:2 and 1:1) by using Digital Image Correlation (DIC) techniques [43]. They found that the Lüders bands can be observed under uniaxial and biaxial tension with a load ratio of 1:2 for aluminium alloy AA5754-O, whereas there are little Lüders bands that can be observed under equi-biaxial tensile conditions. Aytuna et al. studied the mechanical and microstructural effects of PLC band in aluminium 5754 alloy under equi-biaxial and uniaxial conditions by using Scanning Electron Microscopy (SEM), Electron Backscatter Diffraction (EBSD) and DIC [44]. The results show that the PLC effect in the load-time curves seems to be more distinct in uniaxial cases, and the shape of the PLC bands is more sharp and distinct under uniaxial stretching. However, there are diffuse and shifted bands formed under equi-biaxial stretching, which differs from the typical bands with sharp, pronounced, and angled shape.

In the present study, numerical analyses and experiments were carried out to investigate the mechanical response of L450 steel under biaxial loading conditions, and the up-down-up (UDU) model was used to characterize the material performance [45]. The research is organized as follows: Section 2 provides a description of the uniaxial and biaxial loading experiments for L450 steel, as well as the numerical methods used for the up-down-up (UDU) model validation. In section 3, a validation process is carried out by means of uniaxial and biaxial loading experiments: the numerical results are compared with the experimental data in terms of force-time curves and the evolutionary process of Lüders band recorded by Digital image correlation (DIC). Simultaneously, the effect of the displacement loading ratio on the formation of Lüders bands was analyzed by finite element analysis (FEA), revealing the pattern change in the initial band formation. Finally, some conclusions are drawn from this work and these are summarized in section 4. The outcome shows that the effect of biaxial loading on Lüders bands can be evaluated by an appropriate UDU constitutive model validated by uniaxial loading tests.

2. Methodology

2.1. Overview of the approach

The study was carried out in two steps. First, uniaxial loading tests on samples made from L450 steel were carried out, followed by an FE analysis validated by the test results, particularly on the formation and propagation of the Lüders band. In the FE analysis, the UDU model was used as the constitutive model. Different parameters of the UDU model were trialled in the FE analysis, and the parameters leading to the results

closest to the experiment were selected. In the second step of the study, biaxial loading experiments and simulations were carried on cruciform samples made of L450 steel. DIC technique was used to record the strain history on the sample surface, from which details of the Lüders bands can be traced. In the FE analyses, apart from the selected UDU parameters based on the uniaxial loading study, additional variations of the parameters were also tested for a sensitivity analysis, comparing the force-displacement (F-D) curves in both loading directions. Simulations were further expanded to a broad range of loading ratios for a better understanding of the effect of the Lüders plateau, and the formation of the Lüders bands.

2.2. Experimental setup and procedure

2.2.1. Material and uniaxial tests

L450 steel, which is equivalent to API 5L X65 steel, is widely used as a pipeline material in the oil and gas industry. The chemical compositions of L450 steel, as provided by the material supplier, are shown in Table 1.

All uniaxial tests were carried out on an MTS general purpose servo-hydraulic test machine. The tensile rate in uniaxial loading is 2 mm/min, based on published work as well as previous studies to avoid strain rate sensitivity [3,46], following corresponding test standards of GB T 228.1–2010 [47]. The geometry of uniaxial tensile specimens and the stress-strain curve obtained are shown in Fig. 1. Four specimens were tested with consistent results. The stress-strain curve illustrates clearly the Lüders plateau. The mechanical properties of L450 steel are shown in Table 2.

2.2.2. Biaxial tests

Fig. 2 (a) and (b) shows the geometric dimensions and the installation position of the cruciform specimen for biaxial tests. The geometry of cruciform was determined according to the fixture of the MTS biaxial loading machine combined with the information in previous studies [30,48,49]. The biaxial specimens were produced by cutting a thicker steel plate to 3.81 mm thickness into a cruciform using EDM. Four slender through-the-thickness slots were made on each arm to ensure uniform bi-axial loads at the central part. The central circular sags on both sides of specimen are manufactured by electrode erosion. In Fig. 2(a), the thicknesses of the specimen's loading four arms and the circular centre are $t_a = 3.81$ mm and $t_s = 0.81$ mm, respectively. The servo-hydraulic biaxial loading machine was a customer-ordered system from MTS with a capacity of ±100 kN in both directions. All four loading actuators can be independently controlled with alignment functions in both loading directions. Tests were carried out in the vertical position with loading in the horizontal (X) and vertical (Y) directions. Displacement controls (crosshead speeds) were used for tension with equal displacements by opposite actuators. And the centre of the cruciform specimen remained stationary during the test. Force reading was recorded by the load cell at each actuator.

DIC (Model VIC-2D by Correlated Solutions, Inc.) was used to monitor the history of the full-field surface deformation of the cruciform samples. Fig. 3 shows the experimental setup.

Six specimens were tested at room temperature with the loading rate in the Y-direction (V_y) fixed at 1 mm/min. The X-direction loading details corresponding to the specimens are listed in Table 3. DIC data were recorded at a rate of 2 fps. All tests were terminated when unloading had occurred by fracture.

Table 1
Chemical composition of L450 steel (%).

C	Si	Mn	P	S	Al	Cr	Ni	Cu
0.17	0.26	1.48	0.012	0.006	0.021	0.01	0.01	0.01

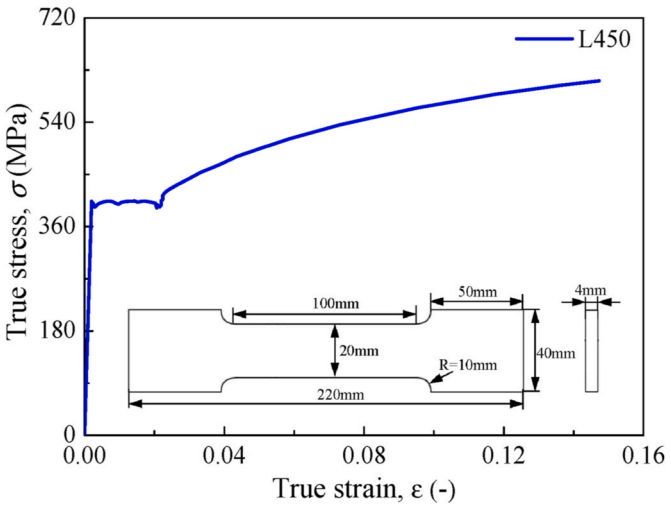

Fig. 1. The stress-strain curve derived from the L450 steel.

Table 2
Mechanical properties of L450 steel.

Young's modulus, E	Upper yield stress, σ_{uy}	Lower yield stress, σ_{uy}	Lüders plateau length, $\triangle e_L$
200 GPa	403.6 MPa	393.5 MPa	2.2%

2.3. Numerical modelling

2.3.1. The constitutive model

The constitutive model used in this study is the so-called up-down-up (UDU) stress-strain response. The model is an isotropic J_2 type elasto-plastic law assuming incremental plasticity and contains a section of strain-softening followed by the conventional strain hardening [3]. Kyriakides and Miller were among the first to use the UDU model in FE analysis to simulate strain localisation due to the Lüders phenomenon [45]. The model is a simplified approach to fit the experimentally determined engineering stress-strain curve that contains a Lüders plateau. In this work, the UDU model was first calibrated with the uniaxial test results to capture the Lüders banding before it was used to simulate the stresses and strains in the biaxial loading conditions.

Fig. 4 illustrates how the UDU fit was constructed based on the uniaxial tensile test curve. The fit consists of three sequential sections, namely ① the linear-elastic range extended to the upper yield stress (s_{uy}) of the UDU model, and ② a linear softening branch, followed by ③ a linear hardening one returning to the test curve. The module is constructed such that the so-called Maxwell stress is equal to the plateau stress (R_{eL}). Corresponding upper and lower yield strengths (s_{uy} and s_{ly}, respectively) are created. A straight line joining these two yield stresses forms two triangles above and below the plateau stress R_{eL}, as shown in Fig. 4 in dashed lines. The areas of the two triangles need to be kept equal, to ensure that energy dissipated during the Lüders phase remains unchanged.

The upper yield stress (s_{uy}) and the lower one (s_{ly}) can be determined by:

$$s_{uy} - R_{eL} = R_{eL} - s_{ly} = \frac{\Delta s}{2} \tag{1}$$

where $\triangle s$ is the difference between s_{uy} and s_{ly}, and is related to the softening modulus (E_L) by:

$$E_L = -\frac{\Delta s}{\Delta e_L} = -\frac{s_{uy} - s_{ly}}{\Delta e_L} \tag{2}$$

where $\triangle e_L$ is the length of the Lüders plateau in terms of the true strain.

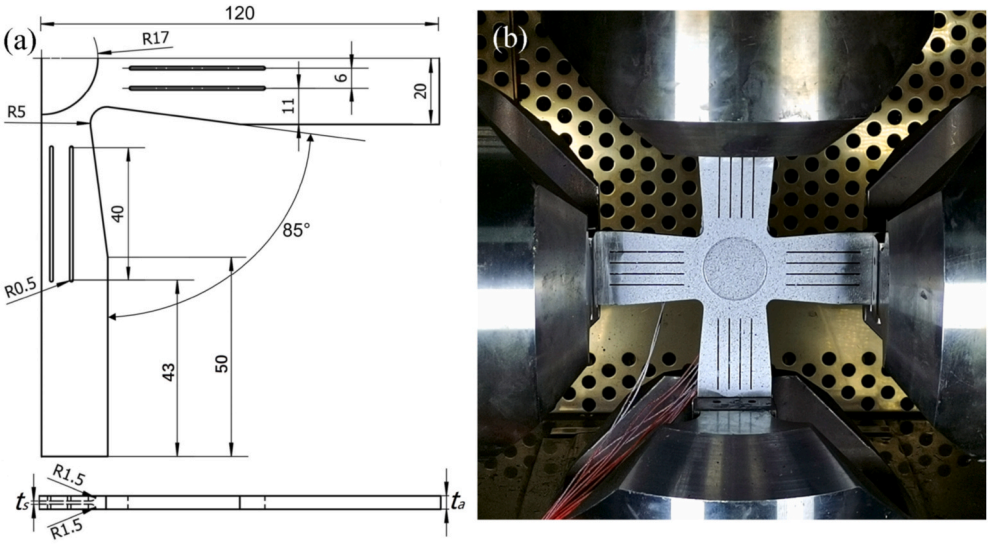

Fig. 2. The biaxial tensile test (a) cruciform specimen geometric dimensioning, (b) the installation position of the cruciform specimen.

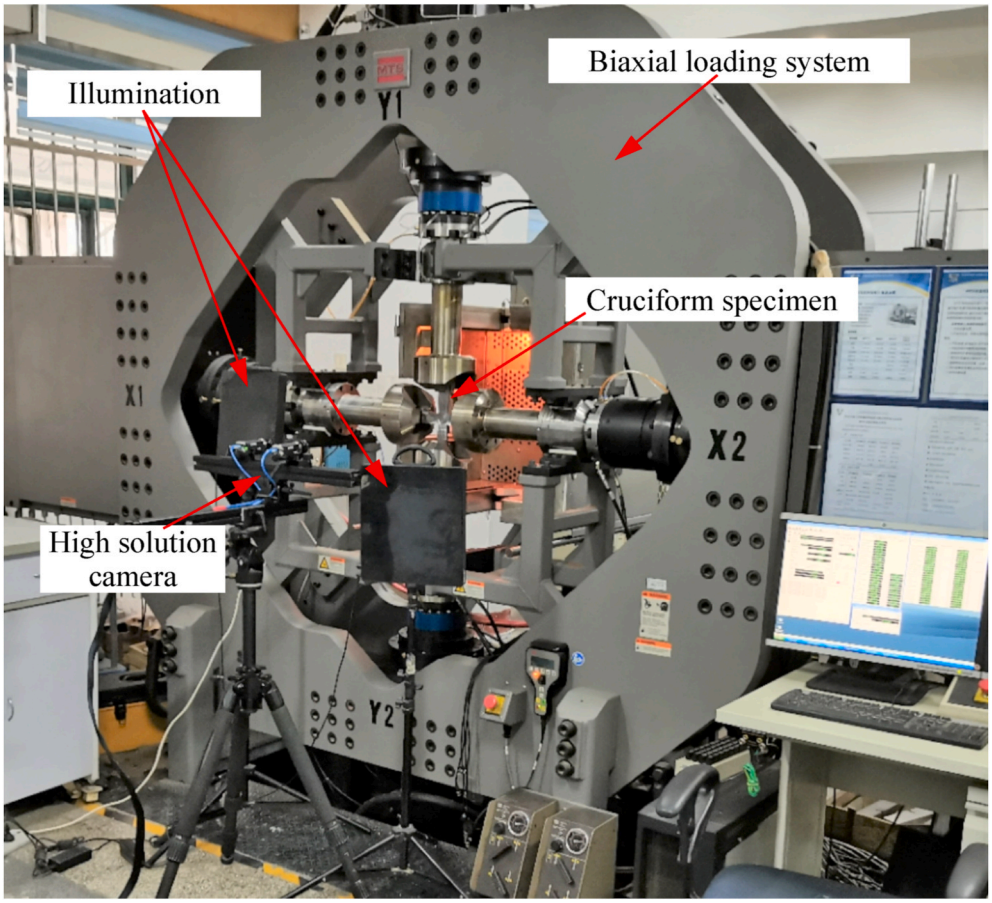

Fig. 3. Experimental set-up of the tensile testing machine with the DIC system.

Fig. 5 shows three normalized softening modulus of UDU models ($\overline{E}_L = |E_L/E|$), leading to different sets of s_{uy} and s_{ly}. Take UDU3 for instance, the upper yield stress s_{uy} and the lower yield stress s_{ly} are 444.43 and 363.23 MPa, respectively. Lüders plateau length $\triangle e_L$ = 2.2%.

The softening modulus E_L:

$$E_L = -\frac{\Delta s}{\Delta e_L} = -\frac{s_{uy} - s_{ly}}{\Delta e_L} = \quad -3690.9\text{MPa}$$

Young's modulus E = 200000 MPa.

The normalized softening modulus $\overline{E}_L$:

$$\overline{E}_L = |E_L / E| = 0.0185$$

Table 3
Biaxial samples and X-direction loading configurations, $V_y = 1$ mm/min.

Specimen	Thickness of loading arms, t_a (mm)	Thickness of central disc, t_s (mm)	Loading rate, V_x (mm/min)
B1-1	3.80	1.14	1
B2-1	3.80	1.15	2
B1-2	3.81	1.24	1
B2-2	3.74	1.24	2
B1-3	3.82	1.24	1
B2-3	3.78	1.11	2

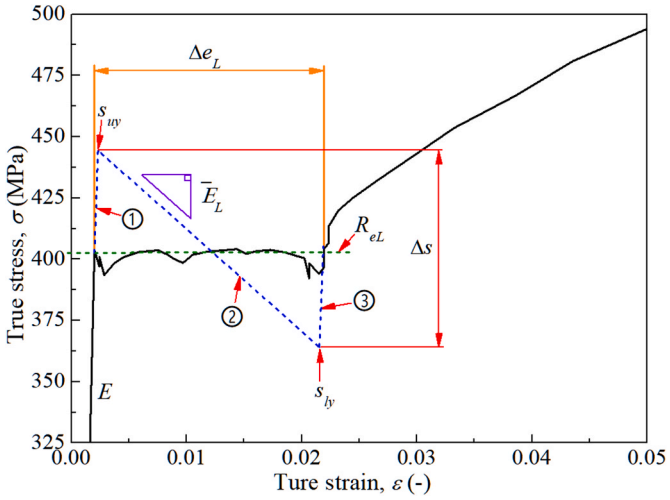

Fig. 4. Illustrative schematic of up-down-up (UDU) stress-strain mode.

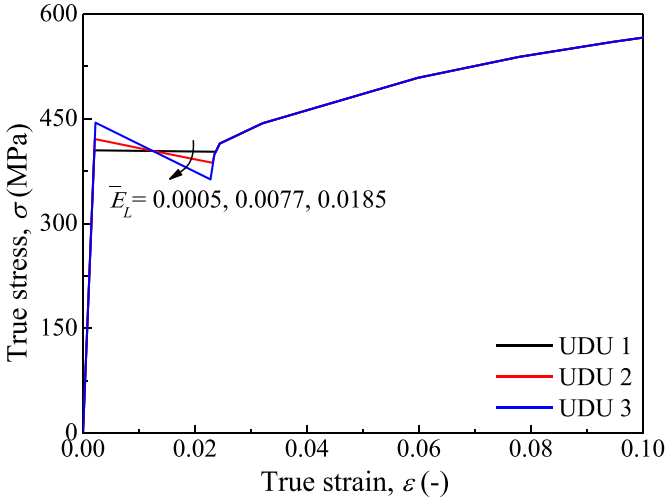

Fig. 5. Constitutive models used in FE analyses.

The purpose is to compare the simulated force-displacement curves based on the UDU models with that of the experiment, so the most suitable model is identified. Parameters of the constitutive models are shown in Table 4. In this study, the UDU curves were imported in ABAQUS by using the material curve.

Table 4
Parameters of material models used in FE analyses of biaxial loading, $E = 200$ GPa, $R_{el} = 403.8$ MPa, $\triangle e_L = 2.2\%$.

Model No.	$\bar{E}_L$	$\triangle s/R_{eL}$
UDU 1	0.0005	0.0050
UDU 2	0.0077	0.0842
UDU 3	0.0185	0.2011

2.3.2. Finite element models

Analyses were carried out using ABAQUS for both uniaxial and biaxial tensile loading processes. All three UDU models discussed above were used for comparison.

2.3.2.1. Uniaxial loading. The FE model is shown in Fig. 6, based on the dimensions of the tensile test specimen in Fig. 1. The left end of the model is fixed, and a displacement loading in the X-direction is applied to the right end of the FE model. The loading position is the reference point coupling with the surface on the specimen thickness direction, the degrees of freedom outside the X direction is constrained to avoid the possible rigid body motion. The code provided element C3D8R (8-node linear brick, reduced integration) was chosen. 1500 elements were found with good convergence to catch the formation of the Lüders band.

2.3.2.2. Biaxial loading. Although the shape and the loading mode are both symmetric for the cruciform specimens, test runs using a quarter and a half model show strain variations at the specimen centre in both models, affecting the formation of the Lüders bands. Hence, a full-scale 3D model was used, as shown in Fig. 7, following the cruciform specimen's dimensions in Fig. 2. Displacement loads of the same value D_x but in opposite directions, and of D_y as well, were applied along the X and Y axes, respectively. A number of ratios between D_x and D_y were studied, as listed in Table 5. The loading position is the reference point coupling with the surface on the thickness direction of specimen arm, the degrees of freedom outside the loading (X or Y) directions are constrained to avoid the possible rigid body motion. Again, element C3D8R was used with sufficient numbers to catch the Lüders band phenomenon, and 18196 elements, with refined mesh in the centre disk region, were used to catch the formation of the Lüders band on the cruciform specimen. Both the element type and mesh density were selected based on mesh-sensitivity analyses.

3. Results and discussions

3.1. Uniaxial loading

The reaction force and the elongation of the gauge length were extracted from ABAQUS outcomes based on the three UDU models. They were converted to true stress-strain curves as shown in Fig. 8(a), together with the experimental curve. Note that these stress-strain curves from the simulations are in an average sense of strain over the sample's gauge length.

All simulation curves are reasonably close to the test one, with visible differences at the beginning of the Lüder's plateau among the three UDU models. It is interesting to see that both the test and UDU3 curves show a recovered "dip" at the end of the plateau, though at slightly different strains, but not for UDU1 and UDU2.

A snapshot of local distributions of the maximum principal strain from FEA and DIC are shown in Fig. 8(b)–8(e) at the global strain of 0.02 when the strain discontinuity appears in the test curve, the lens position limited more results of strain change within the Lüders plateau. The fringe pattern of UDU3 matches best to that of DIC with a band of approximately 45°–55° to the loading axis, which is in agreement with the uniaxial tension results observed by Wang et al. [3].

It appears that UDU3 can best characterize the Lüders plateau of L450 steel under uniaxial tension. Further comparisons were carried out using all three UDU models in simulations of biaxial loading cases.

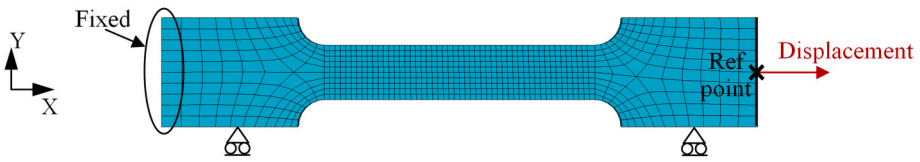

Fig. 6. Mesh and boundary condition used for the dog-bone specimen.

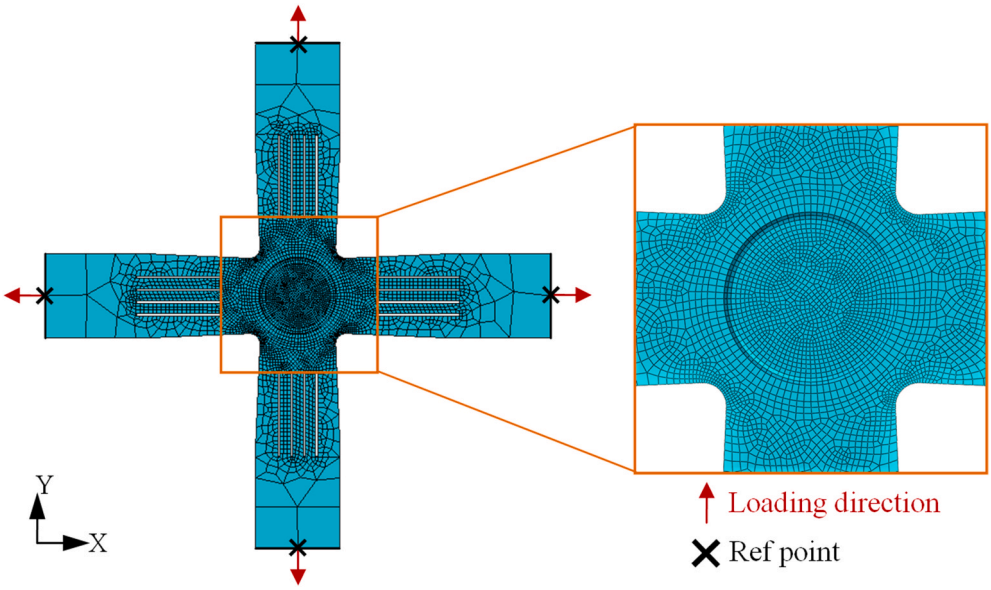

Fig. 7. 3D mesh and boundary condition used for the cruciform specimen.

Table 5
Loading conditions used in biaxial simulations; D_y is fixed at 1 (mm) in all cases.

Specimen	S1	S2	S3	S4	S5	S6(B1-1)	S7	S8	S9
D_x (mm)	FBC[a]	0	0.5	0.6	0.8	1	1.2	1.3	1.4
Specimen	S10	S11	S12	S13(B2-1)	S14	S15	S16	S17	
D_x (mm)	1.6	1.7	1.8	2	3	4	5	10	

[a] Free boundary condition.

3.2. Biaxial loading

3.2.1. Experimental results

The central part of recovered specimens of biaxial tensile tests are shown in Fig. 9 for the loading ratio D_x: D_y at (a) 1:1, and (b) 2:1, respectively. Extended plastic deformation to the stage of necking was observed in all four fillet corners, but only one was cracked for the ratio at 1:1. The crack was initiated and propagated in a K_I mode at 45° to the loading axes.

For the loading ratio at 2:1, necking was seen at all four fillet corners, and two cracks were initiated at the rim of the central disk at 45° locations to the axes but propagated in the perpendicular direction to the X-axis of higher loading. The two cracks finally coalesced into one approximately aligned to the Y-axis. It should be noted that the position of crack initiation is of some random nature depending on variation in the material, dimensions and manufacturing process, etc., though the results and failure phenomenon remain consistent in repeated tests.

The time history of measured forces under different loading ratios are shown in Fig. 10 (a) and (b). The specimens in "B1" and "B2" group show in Table 3 were tested with consistent results.

It shows that the force-time curves in the X and Y axes are almost identical for the ratio at 1:1 in Fig. 10(a). The X-direction curve clearly shows the discontinuity as the Lüders plateau. However, it seems being almost "missed" somehow in the Y-direction curve.

For the loading ratio at 2:1 (Fig. 10(b)), because of the faster displacement speed, the X-direction curve shows higher magnitude with a clear sign of the Lüders plateau, whereas the Y-direction curve show no indication of the plateau.

It is also noted that unloading due to fracture dominates both curves for the ratio at 1:1, but only seen clearly in the X curve for the ratio at 2:1, and slightly in the Y curve. This is due to the final crack in the 2:1 ratio case being vertical to the X axis, yielding in the loss of the load bearing capacity in the direction.

3.2.2. Comparison of strains from FEA and tests

To compare with the DIC results, the principal strains were extracted from FEA outcomes. Figs. 11 and 12 illustrate strain distributions at various times/displacements from the DIC and simulations using the three UDU models for loading ratios of 1:1 and 2:1, respectively. As shown in Fig. 11 for the loading ratio of 1:1, strains first appear at fillets in 45° directions to the loading axes, then spreads out in higher values following the loading increase. But the overall distribution pattern remains the same with the maximum strains in the area along the directions of 45° until the whole central area is in plastic deformation. No fracture was enabled in FE models and simulations were terminated before crack initiation. All three UDU models appear to be able to

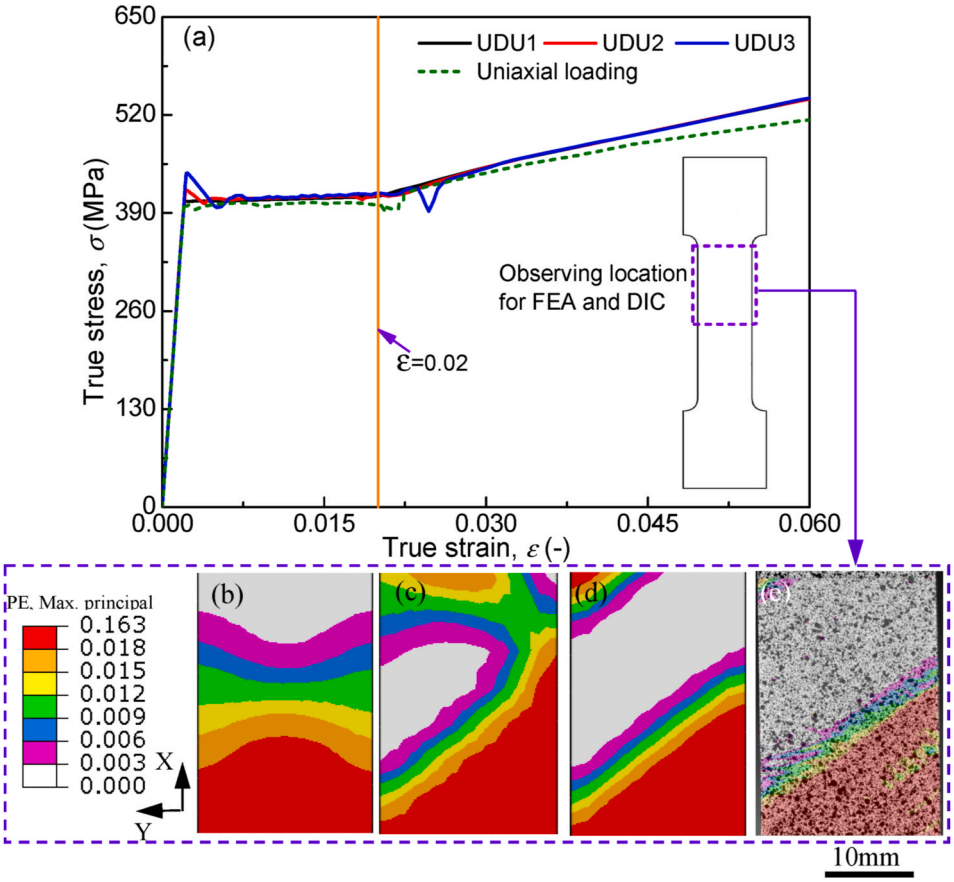

Fig. 8. The changes in plastic strain with the different normalized softening modulus (a) The true stress-strain curve for different normalized softening modulus and uniaxial loading; and (b) UDU1; (c) UDU2; (d) UDU3; (e) DIC for local maximum principal strain distributions at strain = 0.02.

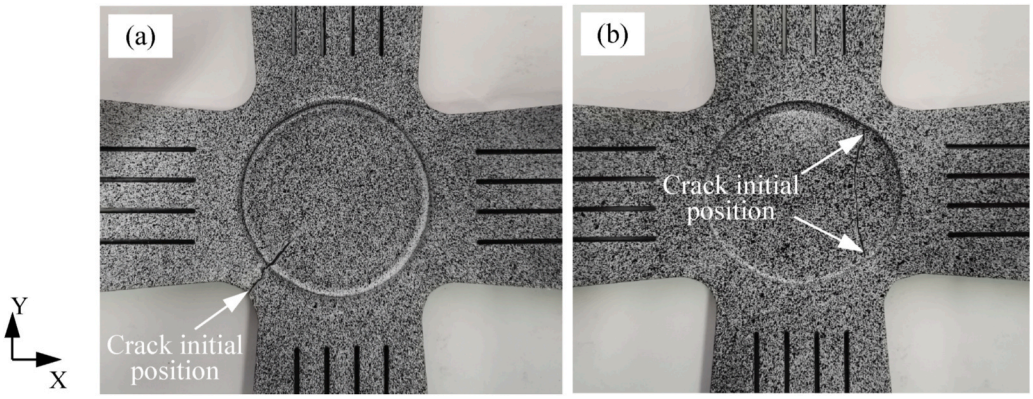

Fig. 9. Biaxial tensile test result (a) Loading ratio D_x: D_y = 1:1; (b) Loading ratio D_x: D_y = 2:1.

capture the key features which are consistent with DIC observations.

Fig. 12 shows the DIC and FEA results under the loading ratio of 2:1. The initial Lüders band was formed at D_y = 0.175 mm. Even though strains at the fillet corners were small, there were two simultaneous bands in the central area by UDU1 and UDU2 at approximately 90° to the X axis, but only one band by UDU3 and DIC at an angle slightly less than 90° to the X axis. With the increasing D_y, a second band appeared on the left-hand side of the central band at D_y = 0.233 mm for UDU3 and DIC, then the third one on the right-hand side at D_y = 0.275 mm to form a triple-band pattern. For UDU1 and UDU2, the double-band pattern remained unchanged in terms of the loading D_y. Finally, at D_y = 0.833 mm the whole central area was taken over completely by plastic deformation.

Based on the above discussion, it can be concluded that UDU3 provides the best match to the DIC results, whereas the other two models show local strain discontinuity that differs from the DIC observation. It is interesting to note that all three UDU models are able to reveal strain concentration positions corresponding to the crack propagation route observed in experiments. One may thus suspect that the Lüders band may affect the direction of crack propagation. It is also worth noting that for the loading ratio of 1:1, no Lüders band was revealed (Fig. 11) by either DIC or simulations of all material models. Minoda et al. [40], Hou et al. [43] and Aytuna et al. [44] also reported similar results for aluminium alloy in their experiments.

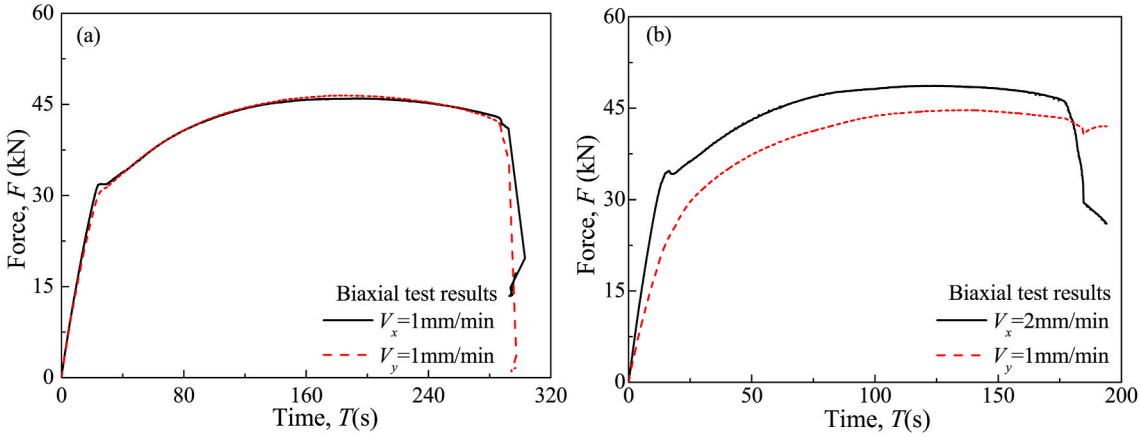

Fig. 10. The force-time curves for same loading ratio (a) D_x: D_y = 1:1; (b) D_x: D_y = 2:1.

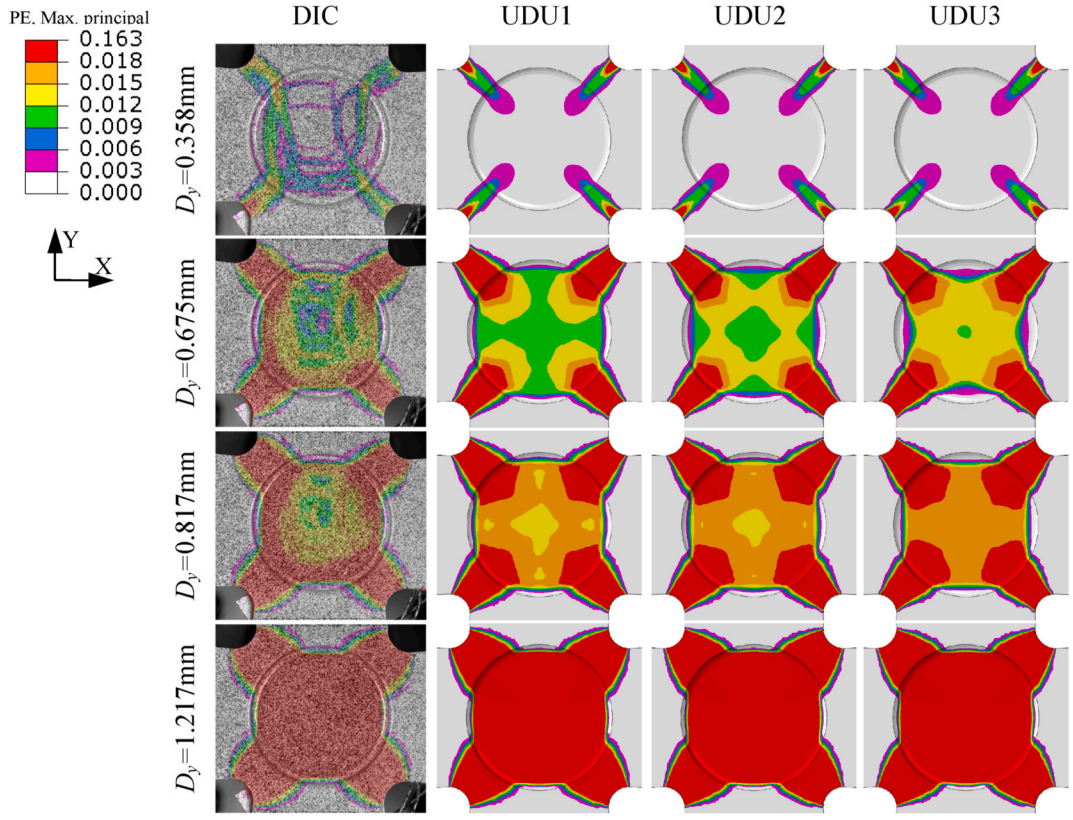

Fig. 11. Comparison of strain development by FEA and DIC for loading ratio D_x: D_y = 1:1.

3.2.3. Comparison of force-displacement curves from FEA (UDU3) and tests

Figs. 13 and 14 illustrate force-displacement curves from experiments (dashed) and FEA (solid), and Figs. 13(a) and 14(a) for zoomed-in details of the Lüders plateau. Note that only model UDU3 was used for better fitting to the DIC results. For the loading ratio at 1:1, FEA results are identical in both X and Y directions, leading to only one curve in Fig. 13. Though there are differences amongst the simulated and measured curves in the elastic and yielding stages, which are likely due to idealised material properties used in simulations and the accuracy of measurement, the overall trend of the curves is similar, revealing clearly the Lüders plateau.

Similar conclusions can be drawn for the loading ratio at 2:1 with the force-displacement curves showing the same trend, though FEA results in the X and Y axes are not identical anymore. Interestingly, like the experimental result, the plateau from FEA appears to be more evidential in the X-direction.

3.2.4. The Lüders band initiation under different loading ratios

To further explore the effect on the initial formation of the Lüders band, the full range of the loading ratio was studied by FEA for a broad picture of the influence.

Fig. 15 shows the distribution of the maximum principal strains under different loading ratios by FEA using UDU3 on the centre disc of the cruciform specimen. Fig. 15(a) shows the case of Y-direction displacement loading only, with the X-direction being set free. The result shows the Lüders band being formed at an angle of approximately 50° to the loading axis (Y-axis). This is consistent with the observation of

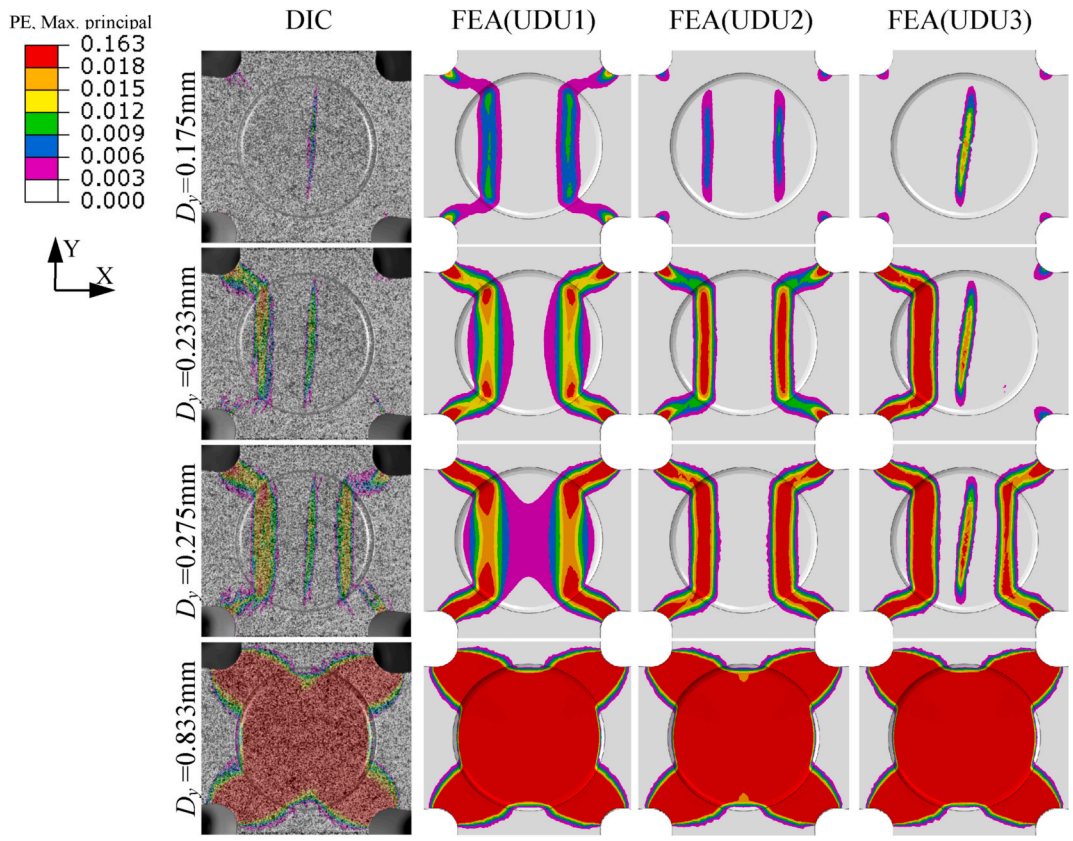

Fig. 12. Comparison of strains from FEA and DIC for loading ratio D_x: D_y = 2:1.

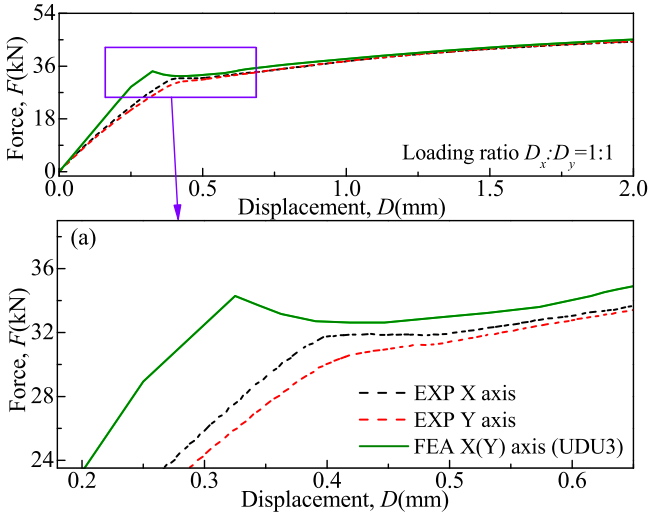

Fig. 13. Comparison of the force-displacement curve from FEA and biaxial tensile test for the loading ratio at D_x: D_y = 1:1.

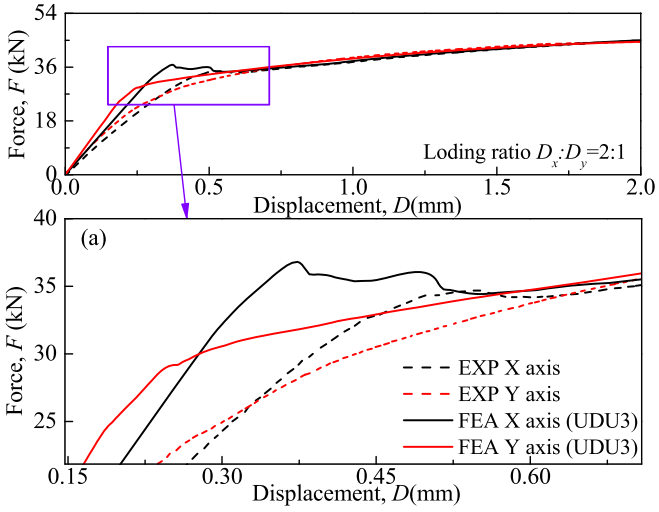

Fig. 14. Comparison of the force-displacement curve from FEA and biaxial tensile test for the loading ratio at D_x: D_y = 2:1.

uniaxial tension experiments by Wang et al. [3]. It should be pointed out that the simulation is in a "pseudo" uniaxial loading consideration, as the free boundary condition in the X axis was set at the "far field" at the ends of the cruciform arms, yielding in some extent of constraints in the X direction in the central part of the cruciform specimen, while a truly uniaxial tensile test using a dumbbell shaped specimens would have the "close field" free boundary condition perpendicular to the loading direction. In comparison, Fig. 15(b) shows the band formation of the case of the loading ratio 0:1, with a "forced" zero displacement condition in the X direction. Despite the "subtle" differences in the loading conditions, there appear to be negligible differences in the initial band formation in the two cases.

Fig. 15(c) to 15(o) show the initial Lüders band or bands under various loading ratios from 0.5:1 to 5:1, respectively. It can be seen that with the exception of the loading ratio 1:1, all the rest of the loading ratios produce some forms of the Lüders band. As discussed in Section 3.2.2, the plastic strain distribution shows an X-shaped pattern in the fillet corners for the loading ratio at 1:1 with no conventional "band" observed.

The overall trend of the band formation, in terms of the loading ratio,

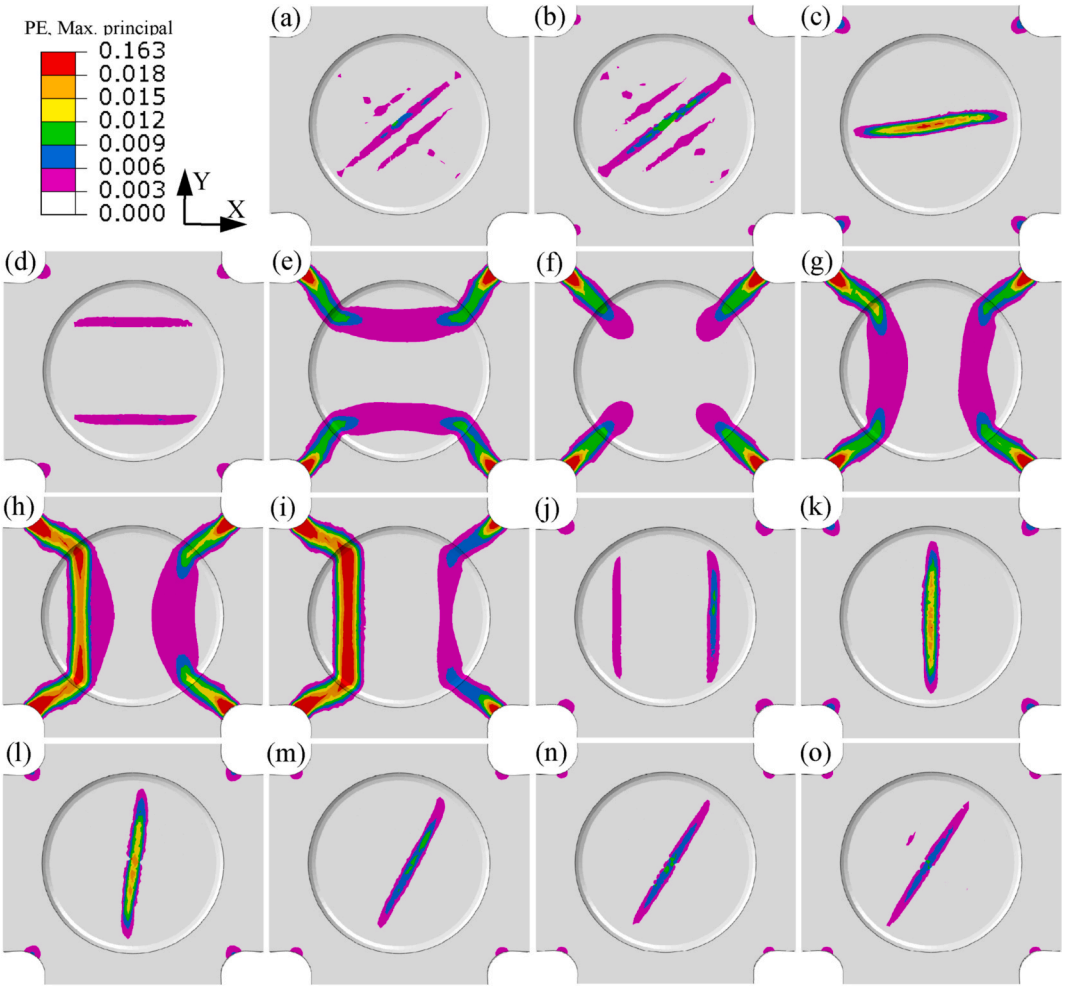

Fig. 15. Relationship between the loading ratio and the Lüders bands (a) free:1; (b) 0:1; (c) 0.5:1; (d) 0.6:1; (e) 0.8:1; (f) 1:1; (g) 1.2:1; (h) 1.3:1; (i) 1.4:1; (j) 1.6:1; (k) 1.8:1; (l) 2:1; (m) 3:1; (n) 4:1; (o) 5:1.

appears to start with an approximately 50° single-band, then a nearly horizontal single-band to a horizontal double-band, then to the X-shaped deformation with "no band", followed by a vertical double-band, and a vertical single-band, then a tilted single-band back to 50°. And the final single-band appears to remain unchanged in terms of higher loading ratios, as a "converging" pattern.

The evolution of the initial Lüders band formation is more clearly illustrated in Fig. 16. The red dash curve shows the angle of the Lüders band measured to the X-axis, and the black solid curve shows the angle to the larger loading axis (i.e. for loading ratios 0:1 to 0.8:1 it is the Y-axis, and for rations 1.2:1 to 10:1, the X-axis). It can be seen that in terms of the loading ratio, the angle of the Lüders pattern to the larger loading axis is almost 50° at the loading ratio at 0:1, then is quickly increased to nearly 90° when the loading ratio is close to 1:1 where there is no band, and is then decreased gradually from 90° to the value same to the uniaxial loading condition. The band number changes from single to double, then no band, to double again, and finally single, in terms of the loading ratios.

3.2.5. *Comparison of FEA force-displacement curves in different loading ratios*

Fig. 17 illustrates the force-displacement curves of different loading ratios leading to single band cases, with (a) for the larger loading axis, and (b) the smaller one, all being FEA results based on UDU3.

Curves in Fig. 17(a) of the higher loading axis shows a clear sign of the Lüders plateau, which is somehow missed in Fig. 17(b) for the

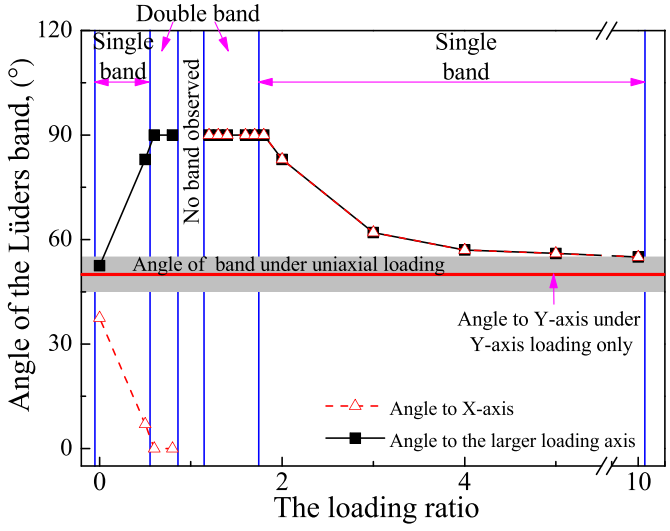

Fig. 16. The angle between the Lüders bands and the larger loading axis under different loading ratios.

smaller loading axis. It appears to indicate that the Lüders plateau would show primarily in the curve of the larger loading direction, and not in the one of the lower loading direction. This is consistent with the

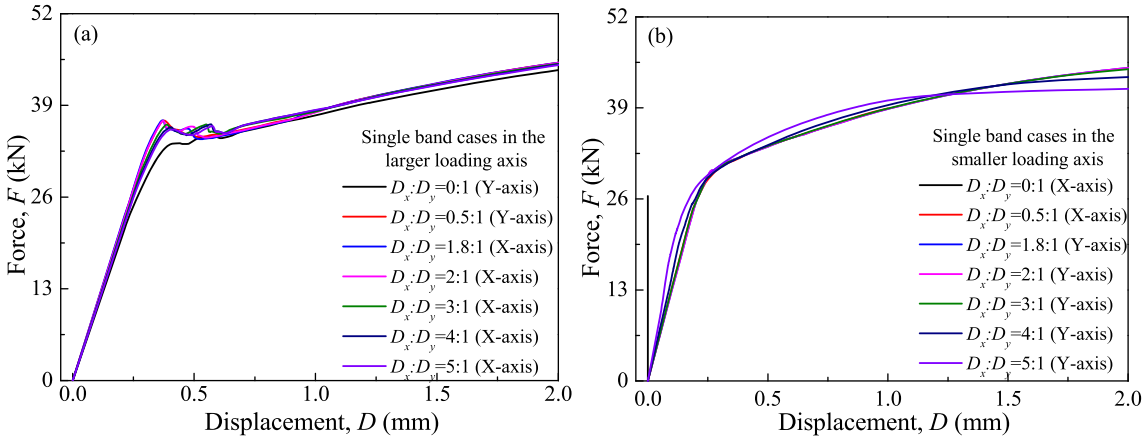

Fig. 17. Force-displacement curves from FEA (UDU3) in (a) the larger and (b) smaller loading axes for single Lüders band cases.

experimental results discussed in section 3.2.3. For Fig. 17(b), note that the vertical line at the distance "zero" is the reaction force in the X-direction under a fixed boundary condition in the X-axis for the loading ratio at 0:1.

For the loading ratios leading to the double-band pattern, Fig. 18(a) and (b) illustrate the force-displacement curves of the larger and the smaller loading axes, respectively. Note that different from Fig. (17), the Lüders plateau can be seen clearly in all curves in Fig. 18(a), and in some in 18(b) to a much less significance.

4. Conclusions

Three-dimensional finite element analysis was carried out on the cruciform specimen under biaxial tension with different loading ratios. The model was verified by DIC data on strain distributions and measured force-displacement curves. Both experiments and simulations reveal that L450 steel shows the Lüders plateau in its stress-strain curve under both uniaxial and biaxial loading conditions.

Having adopted the UDU type of constitutive models to simulate the Lüders plateau, this study demonstrates that the softening modulus of the model has a marked effect on both the mechanical response and the Lüders band formation in terms of the loading ratio. And the Lüders plateau can be appropriately evaluated when the correct UDU constitutive model is chosen. It is found that model UDU3 can best capture the characters of the Lüders plateau for L450 steel.

The biaxial loading ratio has a significant effect on both the number and angle of the Lüders band. Simulations show that with the loading ratio being increased from 0:1 to 10:1, the formation pattern will vary from one of a single-band, to a double-band, then no band, and a double-band, then finally a single-band again. Further increase of the loading ratio will unlikely change the single band mode, as the vast loading difference in the two axes is equivalent to the case of the uniaxial loading.

The angle of the Lüders bands to the larger loading axis also changes in terms of the loading ratio, from approximately 50° (between 45° and 55° in experimental measurement) to nearly 90°, then gradually back to approximately 50°. Note that the loading ratio 1:1 is a special case, where no Lüders band is formed. And for the ratios close to 1:1 (lower or higher), a double-band pattern will form with the angle being 90° (see Fig. 16).

It is observed that the Lüders plateau would appear primarily in the force-displacement curve in the larger loading direction. And this is consistent with both experimental observations and FEA simulations.

The current study has made an effort to gain a better understanding of the stress continuity under biaxial loading conditions, particularly in the formation of the Lüders bands. Though cracks were observed in tests, they appear only after excessive plastic deformation, well after the stage of stress discontinuity at yielding. No attempt has been taken to study the initiation and growth of cracks within the scope of this work. It remains an interesting topic to follow, with relevance to application, such as the structural integrity of pipelines and pressure vessels.

Authorship

Shuai Wang: Investigation, Formal analysis, Data curation, Validation, Software, Writing – original draft, Cheng Hou: Investigation, Data curation, Validation, Bin Wang: Project administration, Conceptualization, Methodology, Supervision, Funding acquisition, Writing – review

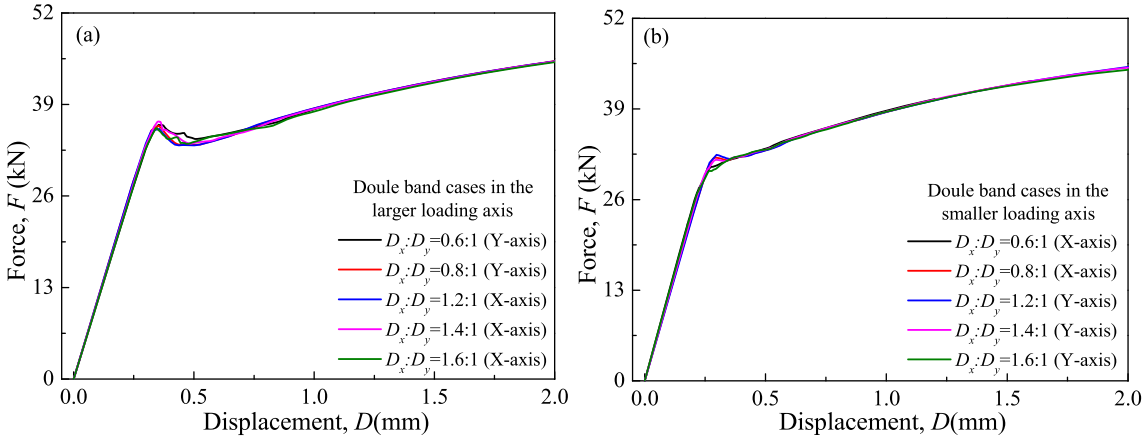

Fig. 18. Force-displacement curves from FEA (UDU3) in (a) the larger and (b) the smaller loading axes for double Lüders bands cases.

& editing, Guiyi Wu: Writing – review & editing, Xueling Fan: Supervision, Funding acquisition, He Xue: Funding acquisition.

Declaration of competing interest

The authors declare that they have no known competing financial interests or personal relationships that could have appeared to influence the work reported in this paper.

Acknowledgements

This work was financially supported by the International Exchanges Programme Scheme project by the Royal Society and National Natural Science Foundation of China (51811530311), Xi'an Jiaotong University State Key Lab for Strengths and Vibration for Mechanical Structures Open Lab Project (SV2017-KF-25), National Natural Science Foundation of China (52075434), Guangdong Basic and Applied Basic Research Foundation (2021A1515110316) and China Scholarship Council (201808610225).

References

[1] Y.G. Cao, Y. Zhen, M. Song, H.J. Yi, F.G. Li, X.Y. Li, Determination of Johnson-cook parameters and evaluation of charpy impact test performance for X80 pipeline steel, Int. J. Mech. Sci. 179 (2020) 105627, https://doi.org/10.1016/j.ijmecsci.2020. 105627.
[2] H. Arabzadeh, M. Zeinoddini, A closed-form solution for lateral indentation of pressurized pipes resting on a flexible bed, Int. J. Mech. Sci. 75 (2013) 189–199, https://doi.org/10.1016/j.ijmecsci.2013.07.003.
[3] L.J. Wang, G.Y. Wu, B. Wang, H. Pisarski, Fracture response of X65 pipes containing circumferential flaws in the presence of Lüders plateau, Int. J. Solid Struct. 156 (2019) 29–48, https://doi.org/10.1016/J.IJSOLSTR.2018.07.027.
[4] C. Soumya, K. Soumyajit, D. Subhankar, S. Mahadev, Role of crystallographic texture, delamination and constraint on anisotropy in fracture toughness of API X70 line pipe steels, Mater. Sci. Eng. 768 (2017) 254–266, https://doi.org/10.1016/j.msea.2017. 09.104.
[5] S. Wang, B. Wang, Y. Janin, R. Bourga, H. Xue, Effects of the surface crack shape on J values along the front of an elliptical crack, Fatig. Fract. Eng. Mater. Struct. 11 (2021) 2944–2961, https://doi.org/10.1111/ffe.13522 (44).
[6] T. Zhao, Z. Tian, New tool for internal pressure during fabrication and installation of mechanically lined pipelines using reel-lay method, Appl. Ocean Res. 58 (2016) 232–240, https://doi.org/10.1016/j.apor.2016.04.009.
[7] Y. Liu, S. Kyriakides, Effect of geometric and material discontinuities on the reeling of pipelines, Appl. Ocean Res. 65 (2017) 238–250, https://doi.org/10.1016/j.apor.2017.04.006.
[8] C. Gupta, J.K. Chakravartty, G.R. Reddy, S. Banerjee, Uniaxial cyclic deformation behaviour of SA 333 GR 6 piping steel at room temperature, Int. J. Pres. Ves. Pip. 82 (6) (2005) 459–469, https://doi.org/10.1016/j.ijpvp.2005.01.005.
[9] H.F. Wang, T.C. Zheng, Z.F. Sang, B.W. Krakauer, Burst pressures of thin-walled cylinders constructed of steel exhibiting a yield plateau, Int. J. Pres. Ves. Pip. 193 (2021) 104483, https://doi.org/10.1016/j.ijpvp.2021.104483.
[10] N. Nourpanah, F. Taheri, Effect of Lüders plateau on fracture response and toughness of pipelines subject to extreme plastic bending, J. Pressure Vessel Technol. 133 (5) (2011), 051701, https://doi.org/10.1115/1.4002930.
[11] T.R. Jacobs, D.K. Matlock, K.O. Findley, Characterization of localized plastic deformation behaviors associated with dynamic strain aging in pipeline steels using digital image correlation, Int. J. Plast. 123 (12) (2019) 70–85, https://doi.org/10.1016/j.ijplas.2019. 07.010.
[12] G. Piobert, A.J. Morin, I. Didion, Commission des principes du tir, Mémorial de l'artillerie 5 (1842) 501–552.
[13] W. Lüders, Uber die Ausserung der Elasticitat an stahlartigen Eisenstaben und Stahlstaben, und uber eine beim Biegen solcher Stabe beobachtete Molecularbewegung, Dingler's Polytechnisches J. (fourth series) 5 (1860) 18–22.
[14] A.H. Cottrell, B.A. Bilby, Dislocation theory of yielding and strain ageing of iron, Proc. Phys. Soc. 62 (1) (1949) 49, https://doi.org/10.1088/0370-1298/62/1/308.
[15] W.G. Johnston, J.J. Gilman, Dislocation velocities, dislocation densities, and plastic flow in lithium fluoride crystals, J. Appl. Phys. 30 (2) (1959) 129–144, https://doi.org/10.1063/1.1735121.
[16] H.B. Sun, F. Yoshida, M. Ohmori, X. Ma, Effect of strain rate on Lüders band propagating velocity and Lüders strain for annealed mild steel under uniaxial tension, Mater. Lett. 57 (29) (2003) 4535–4539, https://doi.org/10.1016/S0167-577X(03)00358-6.
[17] N. Tsuchida, Y. Tomota, K. Nagai, K. Fukaura, A simple relationship between Lüders elongation and work-hardening rate at lower yield stress, Scripta Mater. 54 (1) (2006) 57–60, https://doi.org/10.1016/j.scriptamat.2005.09.011.
[18] H. Louche, A. Chrysochoos, Thermal and dissipative effects accompanying Lüders band propagation, Mater. Sci. Eng. 307 (1–2) (2001) 15–22, https://doi.org/10.1016/S0921-5093(00)01975-4.
[19] S. Kyriakides, A. Ok, E. Corona, Localization and propagation of curvature under pure bending in steel tubes with Lüders bands, Int. J. Solid Struct. 45 (10) (2008) 3074–3087, https://doi.org/10.1016/j.ijsolstr.2008.01.013.
[20] L.J. Wang, E. Eren, B. Wang, G.Y. Wu, Consideration of yield discontinuity in the elastic-plastic fracture analysis of circumferentially flawed pipes, in: Proceedings of ASME 2017 Pressure Vessels and Piping Conference 6A, American Society of Mechanical Engineers, Hawaii, USA V06AT06A035, 2017, https://doi.org/10.1115/PVP2017-65510. Waikoloa, Materials and Fabrication.
[21] J.F. Hallai, S. Kyriakides, On the effect of Lüders bands on the bending of steel tubes. Part I: Experiments, Int. J. Solid Struct. 48 (24) (2011) 3275–3284, https://doi.org/10.1016/j.ijsolstr.2011.06.024.
[22] J.F. Hallai, S. Kyriakides, On the effect of Lüders bands on the bending of steel tubes. Part II: Analysis, Int. J. Solid Struct. 48 (24) (2011) 3285–3298, https://doi.org/10.1016/j.ijsolstr.2011.07.012.
[23] Y. Liu, S. Kyriakides, J.F. Hallai, Reeling of pipe with Lüders bands, Int. J. Solid Struct. 72 (2015) 11–25, https://doi.org/10.1016/j.ijsolstr.2015.07.006.
[24] E. Østby, A.O. Hellesvik, Large-scale experimental investigation of the effect of biaxial loading on the deformation capacity of pipes with defects, Int. J. Pres. Ves. Pip. 85 (11) (2008) 814–824, https://doi.org/10.1016/j.ijpvp.2008.04.009.
[25] Y. Dake, I. Sridhar, X.M. Zhong, S.B. Kumar, Fracture capacity of girth welded pipelines with 3D surface cracks subjected to biaxial loading conditions, Int. J. Pres. Ves. Pip. 92 (2012) 115–126, https://doi.org/10.1016/j.ijpvp.2011.10.019.
[26] R. Rodríguez-Martínez, G. Urriolagoitia-Calderón, G. Urriolagoitia-Sosa, L. H. Hernández-Gómez, E.A. Merchán-Cruz, R.G. Rodríguez-Cañizo, J.M. Sandoval-Pineda, Numerical and experimental analysis of the directional stability on crack propagation under biaxial stresses, J. Phys. Conf. 181 (1) (2009) 12061, 10.10881742-6596/181/1/012061.
[27] K. Ragupathy, K. Ramesh, D. Hall, Effects of negative biaxial loadings and notch on failure assessment diagrams, J. Pressure Vessel Technol. 132 (1) (2010), 011403, https://doi.org/10.1115/1.4000357.
[28] W. Wang, S. Sun, A. Li, S. Zhou, The characteristics of J-integral under biaxial stressing, Int. J. Pres. Ves. Pip. 77 (4) (2000) 159–165, https://doi.org/10.1016/S0308-0161(00)00005-3.
[29] E. Østby, Fracture control-offshore pipelines: new strain-based fracture mechanics equations including the effects of biaxial loading, mismatch, and misalignment, in: ASME 2005 24th International Conference on Offshore Mechanics and Arctic Engineering, 2005, pp. 649–658, https://doi.org/10.1115/OMAE2005-67518.
[30] A. Hannon, P. Tiernan, A review of planar biaxial tensile test systems for sheet metal, J. Mater. Process. Technol. 198 (1–3) (2008) 1–13, https://doi.org/10.1016/j.jmatprotec.2007.10.015.
[31] A. Makinde, L. Thibodeau, K.W. Neale, Development of an apparatus for biaxial testing using cruciform specimens, Exp. Mech. 32 (2) (1992) 138–144, https://doi.org/10.1007/BF02324725.
[32] T. Kuwabara, S. Ikeda, K. Kuroda, Measurement and analysis of differential work hardening in cold-rolled steel sheet under biaxial tension, J. Mater. Process. Technol. 80 (1998) 517–523, https://doi.org/10.1016/S0924-0136(98)00155-1.
[33] V.P. Naumenko, A.G. Atkins, Engineering assessment of ductile tearing in uniaxial and biaxial tension, Int. J. Fatig. 28 (5–6) (2006) 494–503, https://doi.org/10.1016/j.ijfatigue.2005.08.008.
[34] J. Han, C. Lu, B. Wu, J. Li, H.J. Li, Y. Lu, Q. Gao, Innovative analysis of Luders band behaviour in X80 pipeline steel, Mater. Sci. Eng. 683 (2017) 123–128, https://doi.org/10.1016/j.msea.2016.12.008.
[35] J. Petit, G. Montay, M. François, Strain localization in mild (low carbon) steel observed by acoustic emission-ESPI coupling during tensile test, Exp. Mech. 58 (5) (2018) 743–758, https://doi.org/10.1007/S11340-018-0379-2.
[36] J. Ma, H. Liu, Q. Lu, Y. Zhong, L. Wang, Y. Shen, Transformation kinetics of retained austenite in the tensile Lüders strain range in medium Mn steel, Scripta Mater. 169 (2019) 1–5, https://doi.org/10.1016/j.scriptamat.2019.04.044.
[37] A.E. Viard, J. Dirrenberger, S. Forest, Propagating material instabilities in planar architectured materials, Int. J. Solid Struct. 202 (2020) 532–551, https://doi.org/10.1016/j.ijsolstr.2020.05.027.
[38] R.H. Heyer, J.R. Newby, Effects of mechanical properties on biaxial stretchability of low carbon steels, in: 1968 Automotive Engineering Congress and Exposition, 1968, https://doi.org/10.4271/680094.
[39] J. Zhang, Y. Jiang, Lüders bands propagation of 1045 steel under multiaxial stress state, Int. J. Plast. 21 (3) (2005) 651–670, https://doi.org/10.1016/j.ijplas.2004.05.001.
[40] T. Minoda, K. Shibue, H. Yoshida, Influence of stress ratio of biaxial tensile test on the luders band formation in Al-Mg alloy sheets, Mater. Forum 28 (2004) 799–804, https://doi.org/10.2464/JILM.54.110.
[41] J.B. Le Cam, E. Robin, L. Leotoing, D. Guines, Calorific signature of PLC bands under biaxial loading conditions in Al-Mg alloys, in: Residual Stress, Thermomechanics & Infrared Imaging, Hybrid Techniques and Inverse Problems, 2018, pp. 29–35, https://doi.org/10.1007/978-3-319-62899-8_5.
[42] A. Wijler, J.S.V. Westrum, On the difference between lüders bands and portevin - le chatelier bands, Scripta Metall. 5 (10) (1971) 821–824, https://doi.org/10.1016/0036-9748(71)90050-0.
[43] Y. Hou, J. Min, J. Lin, J.E. Carsley, T.B. Stoughton, Plastic instabilities in AA5754-O under various stress states, IOP Conf. Ser. Mater. Sci. Eng. 418 (2018) 12050, https://doi.org/10.1088/1757-899X/418/1/012050.
[44] O.B. Aytuna, M. Efe, Investigation of portevin-LeChatelier bands in 5754 aluminum alloy under various strain paths, Procedia Struct. Integr. 21 (2019) 120–129, https://doi.org/10.1016/j.prostr.2019.12.093.
[45] S. Kyriakides, J.E. Miller, On the propagation of lüders bands in steel strips, J. Appl. Mech. 67 (4) (2000) 645–654, https://doi.org/10.1115/1.1328348.

[46] E. El-Danaf, M. Baig, A. Almajid, W. Alshalfan, M. Al-Mojil, S. Al-Shahrani, Mechanical, microstructure and texture characterization of API X65 steel, Mater. Des. 47 (2013) 529–538, https://doi.org/10.1016/j.matdes.2012.12.031.
[47] Standardization Administration of China, GB T 228.1-2010, China Quality and Standards Publishing & Media Company Limited, 2011.
[48] X. Song, L. Leotoing, D. Guines, E. Ragneau, Characterization of forming limits at fracture with an optimized cruciform specimen: application to DP600 steel sheets, Int. J. Mech. Sci. 126 (2017) 35–43, https://doi.org/10.1016/j.ijmecsci.2017.03.023.
[49] R. Xiao, A review of cruciform biaxial tensile testing of sheet metals, Exp. Tech. 43 (5) (2019) 501–520. https://10.1007/s40799-018-00297-6.